sustainability

Article

Enhancing Cementitious Concrete Durability and Mechanical Properties through Silica Fume and Micro-Quartz

Mohammad Iqbal Khan *, Yassir M. Abbas and Galal Fares

Department of Civil Engineering, College of Engineering, King Saud University, P.O. Box 800, Riyadh 11421, Saudi Arabia; yabbas@ksu.edu.sa (Y.M.A.); galfares@ksu.edu.sa (G.F.)
* Correspondence: miqbal@ksu.edu.sa

Abstract: The existing body of literature has witnessed extensive research efforts dedicated to exploring the impact of supplementary cementitious materials (SCMs) possessing pozzolanic characteristics on concrete. Nevertheless, the holistic concept of micro-scale fillers has frequently been a subject that remains insufficiently explored. This study endeavors to formulate binary cementitious systems that incorporate silica fume (SF) and micro-quartz filler (MQF) to enhance the durability and mechanical properties of cementitious concrete. We systematically investigate the effects of varying replacement levels of SF and MQF, alongside changes in the water-to-binder (w/b) ratio. With w/b ratios spanning 0.25 to 0.40, we explored replacement levels of 8, 10, and 12% (wt.) for SF, and 5, 8, 10, 15, 25, and 35% (wt.) for MQF. The findings revealed a consistent decrease in porosity and permeability as the replacement levels increase. Notably, a marked increase in compressive strength is observed with SF replacement, reaching its peak at an 8% MQF replacement level. Even as MQF replaces 15% of SF, concrete mixtures with 12% SF consistently exhibit superior strength. Importantly, MQF's ultrafine particle size mirrors SF's impact on enhancing compressive strength, porosity reduction, and permeability, despite its high crystalline structure. The study employs an analysis of variance (ANOVA) to rigorously assess the influence of each variable on the studied responses.

Keywords: concrete; micro-quartz; permeability; porosity; silica fume; strength

check for updates

Citation: Khan, M.I.; Abbas, Y.M.; Fares, G. Enhancing Cementitious Concrete Durability and Mechanical Properties through Silica Fume and Micro-Quartz. *Sustainability* **2023**, *15*, 15913. https://doi.org/10.3390/su152215913

Academic Editor: Ramadhansyah Putra Jaya

Received: 8 October 2023
Revised: 8 November 2023
Accepted: 10 November 2023
Published: 14 November 2023

1. Introduction

1.1. Background

Advances in construction technology emerge from the advantages of the latest concrete technology. Since its first use, concrete has become a mandatory gigaton (one billion) material for various construction and structural applications. The estimated worldwide concrete production has reached 30 gigatons [1]. The boom in construction witnessed in the current century has increased the demand for concrete materials, especially cement as the essential binding material. Aïtcin [2] reported that the demand for cement increased from 10 Mt in 1900 to 3.5 Gt until 2016; this increases with the demand for concrete for new constructions. The main ingredients of concrete can be seen as those composing the cementitious matrix and those forming the skeletal aggregates [3–5]. The first phase, the cementitious matrix, is responsible for drying shrinkage and most of the deteriorating reaction when innocuous aggregates are present. The critical zone is represented by the boundaries between the cementitious matrix and aggregate circumferences, which lead to the formation of local stresses along the interface due to shrinkage and hardening processes as weak points [3]. The cracks are well reported to be initiated due to and near these weak points. Accordingly, the overall durability depends on the quality of the interfacial transition zone (ITZ) and its microstructure [6–8]. Therefore, improving the quality of the ITZ becomes a common practice to enhance the durability of concrete. The improvement process can be achieved by reducing the water-to-binder (w/b) ratio and applying appropriate chemical and mineral admixtures, as well as many other fine and ultrafine natural and artificial materials.

1.2. Bibliographical Overview

According to Lagerblad and Kjellsen [9] and Winnefeld [10], the factors affecting the quality of ITZ are the following:

- Type of cement and, accordingly, its chemistry and activity.
- The packing of both the ingredients for the cementitious matrix and aggregate skeleton.
- Chemical and volume stability of the individual cementitious, mortar, and concrete phases.
- A sieve analysis, fineness, and chemical stability of fine and coarse aggregates.

Packing density comes from the main concept of filling the voids in the cementitious matrix using finer powders and those in the aggregate skeleton using well-distributed aggregates. Dispersion becomes critical for optimal packing density, which can be achieved using compatible chemical admixtures. Mineral admixtures with pozzolanic activities contribute to the formation of secondary calcium-silicate hydrates (C-S-H) and other hydration products, depending upon the type of supplementary cementitious material (SCM), which enhances the quality of ITZ. Moreover, the presence of mineral admixtures modifies the flowability of concrete due to the slippage of aggregates, causing it to move from a normal slump to a high degree of flowability. This phenomenon is especially pronounced when employing spherical SCMs, such as fly ash and silica fume (SF). The improved flowability is reported to lead to improved ITZ [11]. The presence of filling particles, either smaller than cement particles or aggregate grains, can be visualized, as shown in Figure 1.

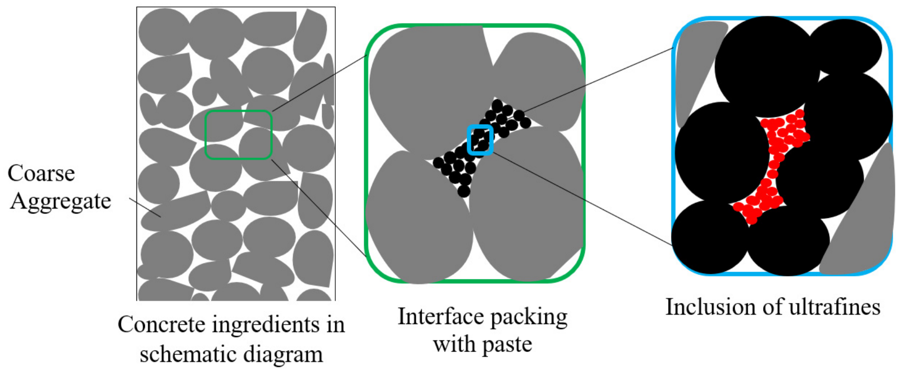

Figure 1. The addition of ultrafine fillers improves the packing of concrete.

The partial replacement of cement with mineral admixtures was shown to have multiple economic and durability benefits. For example, SF has a high degree of pozzolanicity due to its particles with nano-median sizes (200–400 nm) and a high degree of amorphicity [12]. When SF partially replaces cement, it first reduces the amount of cement. It thus reduces the CO_2 footprint, and second, it reacts with the liberated calcium hydroxide (CH) due to the hydration of silicate phases and the formation of C-S-H. This chemical reaction significantly improves the mechanical properties of concrete due to the elevated strength of the cementitious matrix and the enhanced ITZ properties [13–15]. An SF replacement level of up to 15% was reported to be used in the production of high-performance concrete (HPC) with improved strength [16–18]. Compared to the control mixture, the presence of up to 15% SF is also reported to lead to an increase of 21% in the compressive strength that reaches its maximum improvement value at 90 days [16]. Similarly, it is also reported that the incorporation of 6 and 10% SF has led to a 19% and 25% increase in compressive strength, respectively [19]. In another study, the early strength was reduced compared to the control mix due to the presence of SF at low w/b ratios of 0.27 to 0.33 and the improvement was noted after 7 days [20]. The reduction was notable at a higher replacement level. This can be attributed to the difficulty of efficiently dispersing SF at higher dosages, which can also be attributed to the increase in plastic viscosity and yield stress that make the flowability difficult and the packing density lower. All the researchers agreed that the increase in strength could be attributed to the pozzolanicity and filling effect of the nano-sized SF particles.

On the other hand, fly ash (FA) is another type of mineral admixture known for its amorphous alumino-ferrite-silicate structure and especially spherical structures known as cenospheres. Due to the micro-size of its particles, they become slower in the pozzolanic activity with CH compared to SF. Due to the slow pozzolanic activity of FA, its incorporation in a partial replacement of cement causes a notable reduction in the heat of hydration of cement. Therefore, due to its pozzolanic activity and spherical structure, the presence of FA has the dual benefits of secondary hydration and filler [21–26].

For that reason, the effective combination of FA and SF as a partial replacement for cement and an enhancer for strength and durability becomes a common practice [27–35]. The ternary combination of SF (10%) with FA increases its compressive strength compared to the reference binary with FA by about 145% [30]. The ranges of 8–12% SF and 15–20% FA were reported to significantly reduce the permeability and related properties such as porosity and sorptivity [27]. Similarly, it is mentioned that the ranges of 4–8% SF and 20–50% FA could be combined in different ternary mixes for better mechanical properties and the lowest permeability [36]. For example, the combination of 3% SF and 32% FA was found to have a chloride permeability of 3000 coulombs, while it was found to have one below 500 coulombs when formulating 9% SF and 26% FA [37,38]. Therefore, the proportion of binding materials and curing conditions has a substantial effect on the ITZ and durability properties of fillers and materials of variable pozzolanic properties [39–41]. The filler effect due to the size effect can also be attributed to the formation of different nucleation sites that accelerate cement hydration products with condensed and improved microstructures [10,42–45]. Therefore, the packing density at the cementitious matrix and aggregate skeletal levels, in addition to the nature of fine and ultrafine powder, all together represent an overall package that defines the final output's fresh and hardened properties [46–48]. Despite all these old and recent investigations, ultrafine powders, especially silica sand, still need further research.

1.3. Scope and Significance of the Research

In the context of optimizing the ITZ, a critical aspect in concrete, several factors have been extensively investigated [9,10]. These factors include the type of cement and its chemical properties, packing density of the cementitious matrix and aggregate features, as well as the chemical and volume stability of various concrete phases. While the existing literature has primarily focused on the effects of SCMs with pozzolanic properties, the integral concept of micro-scale fillers has often remained underexplored. The enhancement of ITZ quality is intricately tied to optimizing packing density, which relies on achieving efficient dispersion using compatible chemical admixtures. Mineral admixtures like fly ash and silica fume, which possess pozzolanic activities, have demonstrated the potential to modify concrete flowability while contributing to improved ITZ [11]. However, it is important to highlight that the presence of filling particles, notably superfine aggregates, smaller than cement particles or aggregate grains, represents a key aspect that demands further attention. This phenomenon plays a vital role in influencing fresh and hardened properties of concrete and remains a topic that needs additional research. This study aimed to examine the mechanical and durability properties of concrete using different ultrafine fillers and mineral admixtures in binary combinations (i.e., mixes containing SF or MQF with ordinary Portland cement). In this study, we focused on the effects of micro-quartz filler (MQF), in comparison to silica fume, on the properties of various concrete types, including high- and normal-strength concrete mixes. This study examined 40 concrete mixes containing varying ratios of water–binder (0.25, 0.30, 0.35, and 0.40) and binary combinations of both SF and MQF to optimize their strength and durability characteristics. In this comprehensive study, the integration of silica fume and micro-quartz not only innovatively enhances concrete's durability and mechanical characteristics but also positions it as a leading sustainable construction solution.

2. Materials

This study used ordinary Portland cement (PC-type I, which meets ASTM C 150) as the primary binder. Supplementary cementitious material, namely silica fume (SF), was also included. Additionally, micro-quartz (MQF) as ultrafine filler was added to the concrete mixes to improve their strength and durability. It is noteworthy that the MQF was sourced from a local producer renowned for their advanced types of grinders. In this investigation, PC, SF, MQF, and median grain sizes were approximately 13.0, 8.0, 3.5, and 15.0 µm. Table 1 lists the physicochemical properties of the fine powders, and Figure 2a shows their grain size distributions. Figure 2b shows the sieve analysis of crushed fine sand (CFS), natural fine aggregate (NFA), and coarse aggregate (CA), which were obtained from local crushers.

Table 1. The physicochemical properties of the fine powders.

Oxide Composition (%)	PC	SF	MQF
SiO_2	20.2	93.2	99.5
Al_2O_3	5.49	0.2	0.20
Fe_2O_3	4.12	0.03	0.03
CaO	65.43	0.72	0.01
MgO	0.71	0.14	-
Na_2Oeq	0.26	0.07	-
SO_3	2.61	<0.01	-
Loss on ignition (%)	1.38	5.4	-
Specific gravity	3.14	2.27	-
Fineness (m^2/kg)	373	19,000	16,500

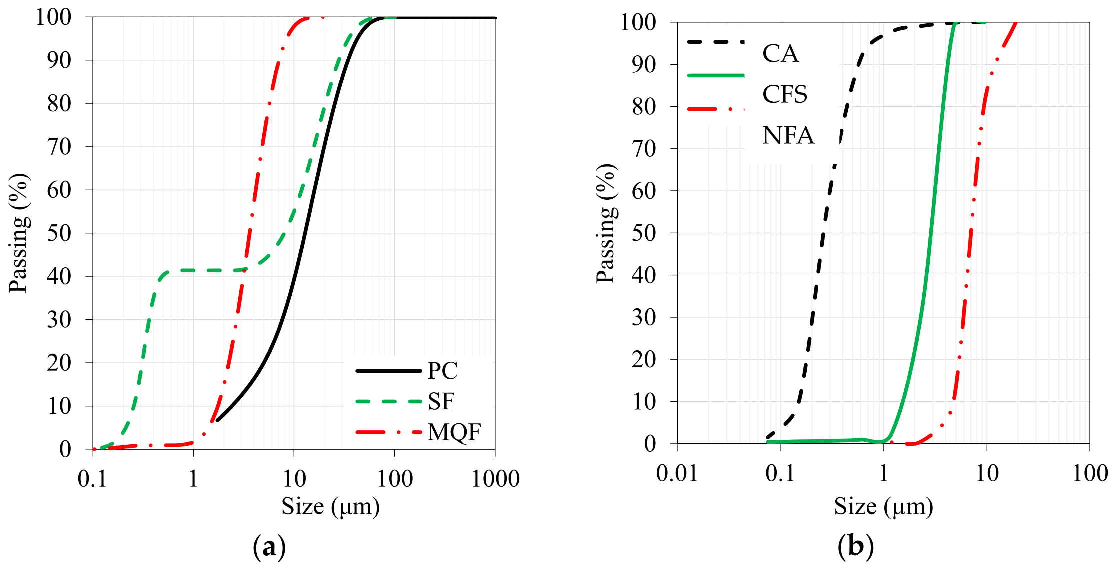

Figure 2. The grain size distribution of (**a**) fine powders, and (**b**) aggregates.

Images of the fine powders obtained with scanning electron microscopy (SEM) are presented in Figure 3. The MQF particles in Figure 3a are characterized by their angular shape, due to grinding, and their average size ranges from 2 to 5 µm. Additionally, Figure 3b illustrates the SEM analysis of the SF, which contained a mixture of smooth- and rough-surfaced condensed sphere particle agglomerates with a mean size of 10 µm, in which a single particle is typically less than 1 µm, according to [49]. Moreover, Figure 3c illustrates the PC particles with polyangular and asymmetrical sizes, and ranging in size from 1 to 20 µm.

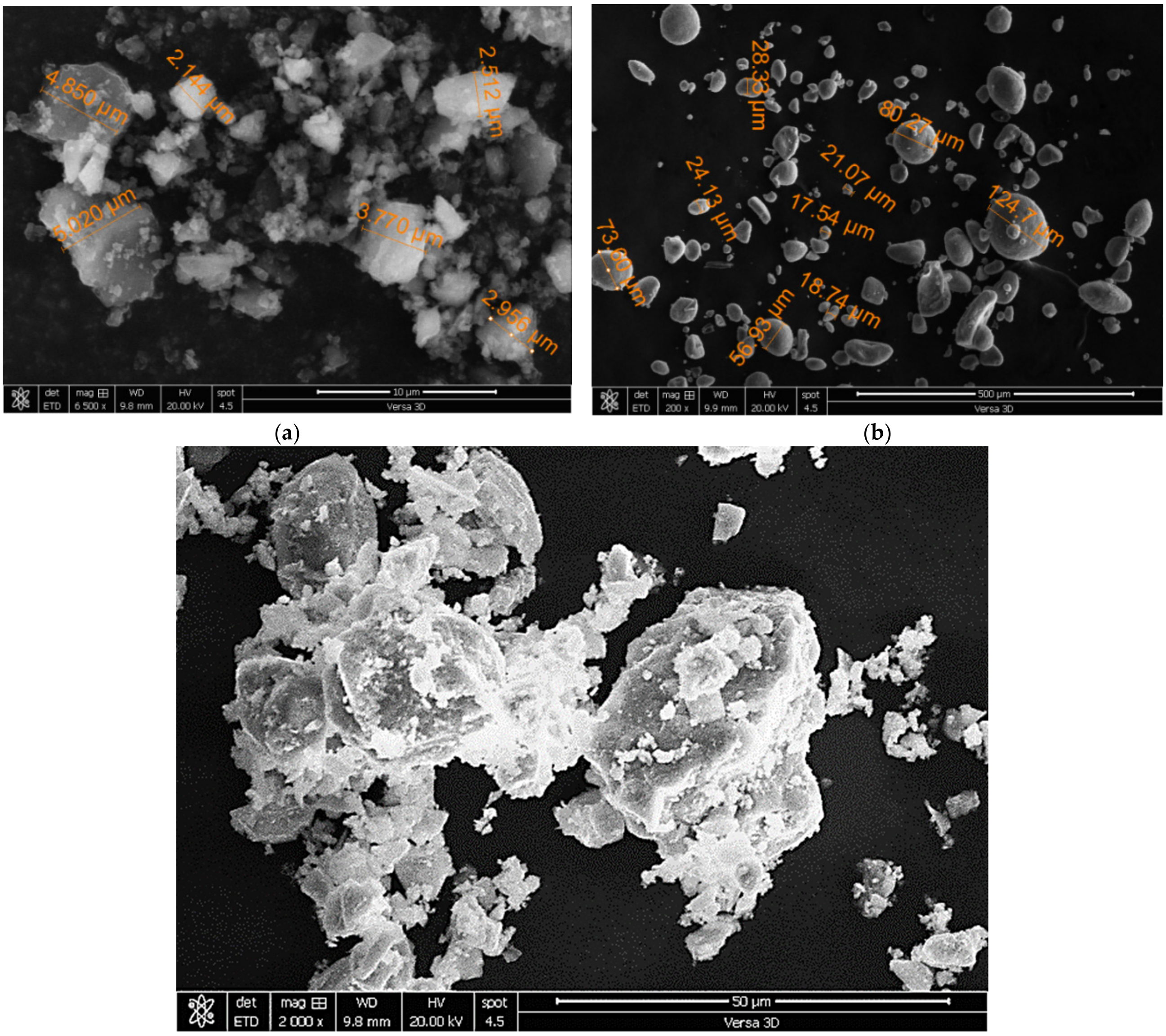

(**a**) (**b**) (**c**)

Figure 3. SEM images of (**a**) MQF, (**b**) SF, and (**c**) PC.

This study utilized a modified polycarboxylic ether polymer superplasticizer (SP) known as Glenium 51 to achieve the required workability of concrete mixes. The dry extract of this soluble compound is 36%, and it exhibits a specific gravity of 1.1. To express the SP dosage in the binder content of the concrete mixture, a ratio of the dry extract (D.E.) and the cement weight (%, wt.) was divided, and this ratio was optimized for a concrete mixture that would provide the highest workability. In this investigation, we used two types of sand with varying particle sizes to prepare the concrete mixes, CFA and NFA. These fine aggregates were characterized by fineness moduli of 4.66 and 1.47, respectively. In the blended fine aggregates, the fineness modulus was 2.54 as a result of the combination of 65% NFA and 35% CFA. Furthermore, CA with an aggregate size of not more than 10 mm was also used in the preparation of all concrete mixtures. Figure 2b illustrates the grain size distribution of the aggregates, while Table 2 summarizes their physical properties.

Table 2. The physical properties of the aggregates.

Material	Specific Gravity	Absorption, %	Unit Weight, kg/m^3
NFA	2.63	0.77	1725
CFA	2.68	1.52	1552
CA	2.65	1.45	1570

3. Methodology

3.1. Detail of Mixes

This study examined 40 concrete mixes containing SF and MQF to determine the optimal mixture for strength and durability. Table 3 displays a detailed breakdown of these different mixes' water–binder ratios and fine powder contents. CTRL refers to the control mixes, while the mixes with SF and MQF were identified by SF and MQF prefixes, followed by the replacement level. The CA content for all 40 mixes was 1056 kg/m^3, while the total FA content of these mixes was 450 $\pm$ 40 kg/m^3. The SP for these mixes ranged from 4.3 to 12.6 L/m^3, which was adjusted to maintain the slump (measured in accordance with ASTM C 143) within a reasonable range (175 $\pm$ 25 mm). A notable feature of the concrete casting process is the measurement of the unit weight of the concrete to determine its fresh density, as per ASTM C138. The measurements of these mixes with unit weights range from 2361.4 to 2481.4 kg/m^3, with a mean value of 2418.4 kg/m^3.

Table 3. Details of concrete mixes.

Sr. No.	Mix ID	w/b	Fine Powders			
			PC	SF	MQF	Total
			(kg/m^3)			
1	CTRL-25	0.25	550	-	-	550
2	SF08-25		506	44.0	-	550
3	SF10-25		405	45.0	-	550
4	SF12-25		484	66.0	-	550
5	MQF05-25		523	-	27.5	550
6	MQF08-25		506	-	44.0	550
7	MQF10-25		405	-	45.0	450
8	MQF15-25		468	-	82.5	550
9	MQF25-25		413	-	137.5	550
10	MQF35-25		358	-	192.5	550
11	CTRL-30	0.30	500	-	-	500
12	SF08-30		460	40.0	-	500
13	SF10-30		360	40.0	-	400
14	SF12-30		440	60.0	-	500
15	MQF05-30		475	-	25.0	500
16	MQF08-30		460	-	40.0	500
17	MQF10-30		360	-	40.0	400
18	MQF15-30		425	-	75.0	500
19	MQF25-30		375	-	125.0	500
20	MQF35-30		325	-	175.0	500

Table 3. *Cont.*

Sr. No.	Mix ID	w/b	Fine Powders			
			PC	SF	MQF	Total
			(kg/m^3)			
21	CTRL-35	0.35	450.0	-	-	450
22	SF08-35		414.0	36.0	-	450
23	SF10-35		495.0	55.0	-	550
24	SF12-35		352.0	48.0	-	400
25	MQF05-35		427.5	-	22.5	450
26	MQF08-35		414.0	-	36.0	450
27	MQF10-35		495.0	-	55.0	550
28	MQF15-35		382.5	-	67.5	450
29	MQF25-35		337.5	-	112.5	450
30	MQF35-35		292.5	-	157.5	450
31	CTRL-40	0.40	400.0	-	-	400
32	SF08-40		368.0	32.0	-	400
33	SF10-40		450.0	50.0	-	500
34	SF12-40		396.0	54.0	-	450
35	MQF05-40		380.0	-	20.0	400
36	MQF08-40		368.0	-	32.0	400
37	MQF10-40		450.0	-	50.0	500
38	MQF15-40		340.0	-	60.0	400
39	MQF25-40		300.0	-	100.0	400
40	MQF35-40		260.0	-	140.0	400

3.2. Mixing, Casting, and Curing

The current mixing procedure, with its adherence to ASTM C192, has been widely adopted in various research endeavors. In this study, the various aggregates were stirred in a typical concrete mixer for a few minutes while the associated absorption water was introduced simultaneously. Afterward, the fine powders were mixed dry for a few minutes to ensure uniformity. Then, the mixing water and SP solution were combined as a ready-mixed blend and stirred for 3 min, followed by a 3-min break and a second 2-min stir. As in this case, the mixing process continued until a homogenized mixture had been achieved, practically within 2 to 5 min. Finally, the mixer was turned off, and the specimens were cast into the molds, which concluded the mixing process. In Table 4, detailed characteristics of specimens cast from different cement-based materials are presented to assess their properties. To maintain the specimen's moisture condition, a trowel was used to smooth the top surface and a plastic sheet was placed to cover it. In this investigation, the following curing method was employed. Standard curing (according to ASTM C31): The specimens were cured in a humidified environment (at 22 °C and 100% RH).

Table 4. Detail of the cylindrical specimens for material testing.

Test	Uniaxial Compression	Rapid Chloride-Ion Permeability
Specimen dimensions (mm)	$D = 100$ $L = 200$	$D = 50$ $L = 100$

3.3. Testing Procedures

3.3.1. Uniaxial Compression Test

A thin layer of sulfur mortar was applied to the cylindrical specimens before performing the uniaxial compression test, as per ASTM C617. This ensures that the top and bottom surfaces are flat, thus ensuring the load will be equally distributed. In this study, the 28 d elasticity modulus and the compressive strength of cement-based materials were assessed according to the specifications of ASTM C469 and ASTM C39, respectively. The test was conducted on a ToniTech universal compression testing machine (capacity of 3000 kN, see Figure 4). Two linear variable displacement transducers (LVDTs) and compressometer rings were attached at approximately 100 mm (the center height of the samples) to quantify in-plane and transverse strains. The loading conditions in this study were displacement- and load-controlled (i.e., 2.5×10^{-3} mm/s and 0.25 MPa/s, respectively). We conducted the measurements for two or three duplicates of the compression test samples in order to ensure reliability, while the mean result is reported. In the majority of instances, the mean was determined based on two specimens, although a third specimen was incorporated when lower repeatability was detected.

Figure 4. The uniaxial compression test: (**a**) schematic diagram and (**b**) testing setup.

3.3.2. Rapid Chloride-Ion Permeability Test

Following ASTM C1202, we performed a chloride permeability test on concrete cylinders with diameters of 50 mm and lengths of 100 mm. As recommended by RILEM [50], these cylindrical concrete samples were vacuum-soaked to maintain continuous saturation levels. In terms of analyzing diffusion characteristics, the chloride permeability test does not provide an accurate measure of these characteristics [33]. Nevertheless, this test can be used to examine parametric data in the context of this study such as the effect of the w/b ratio, replacement level, and type of additive. Figure 5 illustrates how concrete cylinders are filled with chloride before the test is conducted in order to measure the concrete's chloride permeability. We conducted the measurements on two or three duplicates of the chloride permeability sample in order to ensure the reliability and repeatability of the results of this study.

3.3.3. Porosity Test

In this study, concrete's porosity was evaluated in accordance with RILEM CPC 11.3. To accomplish this test, a disc concrete specimen (100 mm diameter with 50 mm height) was dried at 100 ± 5 °C until a constant weight was obtained. We placed dried concrete samples under a vacuum in a desiccator for 3 h, then immersed them in de-aired distilled water for another hour, followed by an additional immersion in the desiccator. Accordingly, we were able to calculate an estimate of the total porosity of concrete as a result of Equation (1).

$$\text{Porosity}(\%) = \left[\frac{M_3 - M_1}{M_3 - M_2}\right] \times 100 \tag{1}$$

where M_3 is the mass of the water-saturated concrete specimen in air, M_1 is the mass of the oven-dried concrete specimen, and M_2 is the mass of the concrete specimen in water.

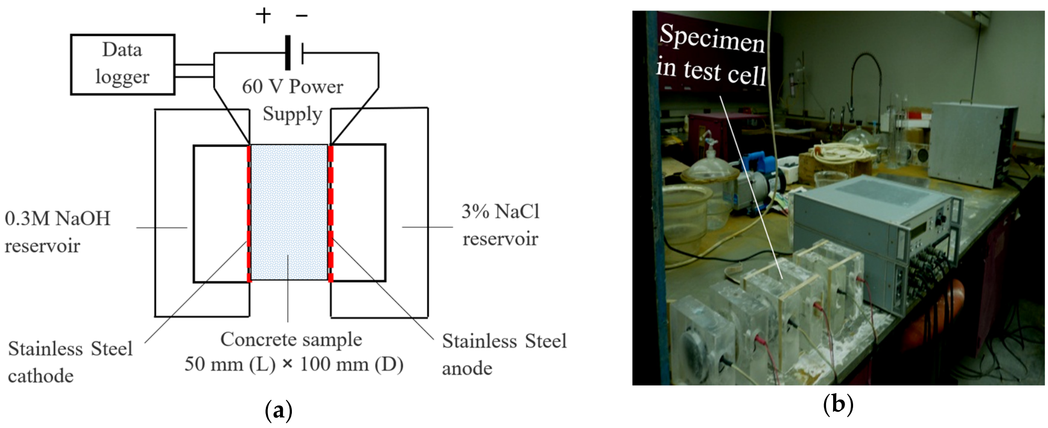

Figure 5. Rapid chloride-ion permeability test: (**a**) schematic diagram and (**b**) testing setup.

4. Results and Discussion

The results of the experiments conducted in this study are summarized in Table 5. In the following sections, we will discuss the results of the experiment in more detail.

Table 5. Summary of the experimental results.

Mix ID	Strength (MPa)				Porosity %	Permeability Coulombs
	7 d	28 d	180 d	400 d		
CTRL-25	70.4	89.9	93.0	96.0	7.9	1433.3
MQF05-25	71.6	91.7	95.5	101.0	7.0	1169.0
MQF08-25	74.1	93.4	97.4	105.3	6.3	893.7
MQF10-25	68.8	85.8	90.9	95.8	5.4	699.3
MQF15-25	64.7	80.8	88.7	96.1	4.7	460.0
MQF25-25	51.6	77.3	86.7	93.9	3.0	97.7
MQF35-25	49.0	70.9	85.6	92.2	2.7	61.7
SF08-25	66.7	91.8	94.4	97.1	4.2	332.7
SF10-25	69.0	94.9	95.9	97.9	3.6	235.3
SF12-25	72.1	98.1	98.2	99.3	3.1	150.0
CTRL-30	60.4	77.7	83.9	88.6	8.1	2400.7
MQF05-30	62.0	80.0	84.1	92.1	7.6	1502.3
MQF08-30	63.4	81.4	87.1	96.9	7.0	885.7
MQF10-30	57.4	75.4	82.4	89.9	6.2	753.3
MQF15-30	53.1	68.8	78.6	88.7	5.9	553.3
MQF25-30	44.1	67.5	75.5	84.7	5.2	167.0
MQF35-30	41.9	61.5	72.3	81.4	4.3	89.7
SF08-30	57.8	79.5	80.9	83.9	5.5	413.7
SF10-30	59.4	81.7	85.2	86.9	5.3	332.7
SF12-30	62.8	86.4	87.1	88.0	4.0	312.7

Table 5. *Cont.*

Mix ID	Strength (MPa)				Porosity %	Permeability Coulombs
	7 d	28 d	180 d	400 d		
CTRL-35	52.7	69.5	74.9	79.4	9.2	2814.7
MQF05-35	53.8	71.8	80.8	84.4	8.8	1936.7
MQF08-35	55.5	74.3	85.0	90.2	8.6	1406.0
MQF10-35	50.5	63.8	75.3	78.5	8.0	1125.0
MQF15-35	49.3	57.8	68.0	74.1	7.5	997.5
MQF25-35	40.0	54.6	63.1	72.1	6.6	544.7
MQF35-35	34.3	49.8	56.4	65.9	6.5	296.7
SF08-35	54.1	73.6	75.0	80.1	6.7	523.0
SF10-35	53.2	74.2	77.4	83.3	6.3	483.0
SF12-35	56.7	77.8	78.4	75.5	6.1	423.7
CTRL-40	46.7	59.2	61.8	65.4	11.3	3437.0
MQF05-40	48.0	61.0	66.2	71.1	10.2	2453.0
MQF08-40	49.9	63.2	69.2	76.1	9.6	1886.7
MQF10-40	43.6	53.7	60.4	65.7	8.9	1404.0
MQF15-40	39.7	49.6	58.7	64.2	8.5	1080.3
MQF25-40	31.6	44.8	53.8	60.8	8.0	847.0
MQF35-40	28.9	42.8	50.5	60.0	7.2	323.0
SF08-40	47.8	64.2	67.8	72.9	7.4	851.3
SF10-40	48.0	65.6	69.5	74.5	7.1	782.7
SF12-40	51.0	69.9	70.9	71.8	6.9	740.0

4.1. *Strength Characteristics*

4.1.1. The 28 d Compressive Strength of SF and MQF Concrete

Figures 6 and 7 illustrate the influence of MQF and SF on the 28 d compressive strength of concrete mixes developed with a variety of water–binder ratios (0.25, 0.30, 0.35, and 0.40). Figure 6 shows that compression strength was almost unaffected with ultrafine replacement rated at less than 8% in the concrete matrix regardless of the water–cement ratio. We also noticed that compressive strength increased slightly when 8% of cement was replaced with ultrafine material. The 28 d's compressive strength decreases, however, if the ultrafine dosage reaches 10% or more. In the presence of increasing water–binder ratios, this decrease in compressive strength became more apparent. In the case of the 0.4 water–cement ratio, the 28 d strength was reduced by 10, 16, 24, and 28% for MQF replacement levels of 10, 15, 25, and 35%, respectively. The elevated crystallinity of the MQF may explain this reduction in compressive strength. Once the filling effect shown with the optimal replacement level is surpassed, the additional levels cause a dilution effect with reduced strength. The presence of micro-packing effects could explain the lack of reductions or even slight increases at low MQF doses. A noteworthy aspect of this conclusion is that it agrees with the conclusions from prior studies [51–55].

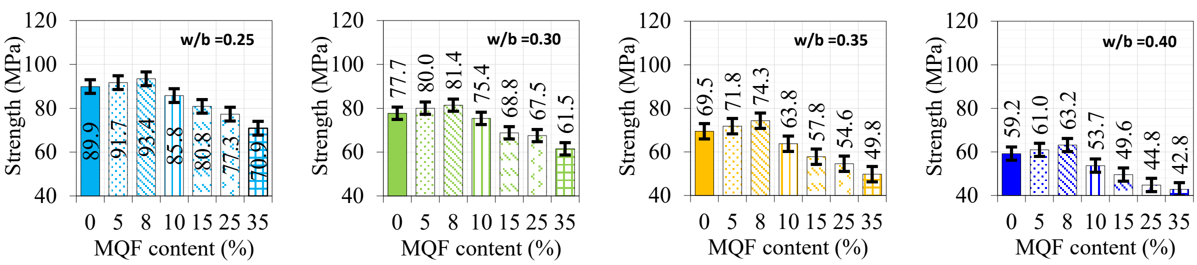

Figure 6. The impact of the MQF content on the 28 d compressive strength.

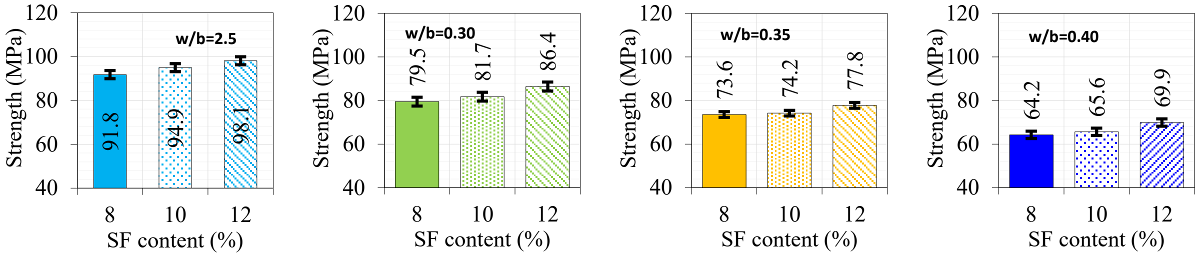

Figure 7. The impact of the SF content on the 28 d compressive strength.

Typically, silica fume is used to enhance the properties of cement-based materials; therefore, it is used predominantly in high-performance concrete due to its fineness and pozzolanic reaction. Figure 7 illustrates the 28 d compressive strength of concrete has been increased with the addition of 8, 10, and 12% SF for four different ratios of water–binders (0.25, 0.3, 0.35, and 0.4). The enhanced compressive strengths of the mixes with a w/b ratio of 0.25 and SF replacement levels of 8, 10, and 12% were 2, 5, and 9%, respectively. While those at w/b ratios of 0.3 were 3, 5, and 11%, respectively. Similarly, the improvements in strength at a w/b ratio of 0.35 were 8.5, 11, and 18%, whereas those at a w/b ratio of 0.40 were 8, 10, and 12%, respectively. There have been several studies stating that concrete strength can increase by 30 to 100% depending on many factors such as mix type, cement type, SF dosage, superplasticizer, aggregates, and curing regime [56–59]. In concrete, SF particles improve packing by filling in the spaces between the particles. In the same way, they fill gaps between coarse aggregates when they are mixed with cement. These findings showed that the maximum 28 d strength of concrete (18%) was obtained with 12% SF and a 0.4 water–binder ratio. As the water–binder ratio increases, the incorporation of SF appears to be more effective at enhancing concrete strength. The higher the water–binder ratio, the more porous the concrete becomes, which makes SF an extremely valuable component of increasing strength due to its micro-filling effect. It is true that concrete has a low water–binder ratio, like that of 0.25 or 0.30, and is pretty compact, but the fine particles still contribute to the strength of the mix. The major role the SF would play in a scenario like this would be to enhance the flowability of the concrete during its plastic phase. It has been scientifically proven that filling the spaces between cement grains occurs whenever there is sufficient SP available to counteract the electrostatic forces between the particles of cement [60,61].

4.1.2. A Modified ABRAM's Model for SF and MQF Concrete

In the second decade of the 20th century, Abram [62] developed a relationship between the compressive strength and the water–cement ratio of normal concrete, as represented with Equation (2), where $A = 96.6$ and $B = 8.2$ [63,64]. The development of this relationship was considered a significant step in concrete technology [63]. There are a number of factors that contribute to the strength of concrete. The factors are classified by Newman [58] into three categories: (i) properties and ingredients of constituent materials, (ii) curing system, and (iii) testing parameters. In order to understand how concrete responds to stress, various factors must be understood. It is therefore essential to formulate an exact formula for the prediction of the compressive strength of any modified concrete in order to determine its strength. In the present study, a modification factor (α) is introduced into Abram's formula (Equation (3)). This modification factor was calculated using the most closely fitting experimental data for all mixtures.

$$f_c' = \frac{A}{B^x} \tag{2}$$

$$f_c' = \alpha \frac{A}{B^x} \tag{3}$$

where,

f'_c: the concrete's compressive strength at a certain age (here, considered 28 d).
A and *B*: the empirical-based factors reflect the effects of individual constituent materials, the curing system, testing parameters, and the age of concrete.
x: the water–binder ratio.

Figure 8 shows the prediction capacity of the proposed formula (Equation (3)) for the water–binder and 28-day compressive strength of MQF and SF concrete's strength relations. The alpha value for the MQF concrete was determined to be 1.32, whereas the alpha value for the SF concrete was determined to be 1.60. Figure 8a illustrates that most MQF concrete points fall within the error range of ±15%, in contrast to Abram's formula (Equation (2)), which underestimated concrete strength. In addition, Figure 8b reveals that SF concrete data points fall within the ±5% error band of the proposed model, while Abram's distinctly underestimates it. Abram's model, initially developed for designing plain concrete, may be conservative because concrete with micro-fillers typically achieves higher compressive strength due to improved particle packing and reduced porosity.

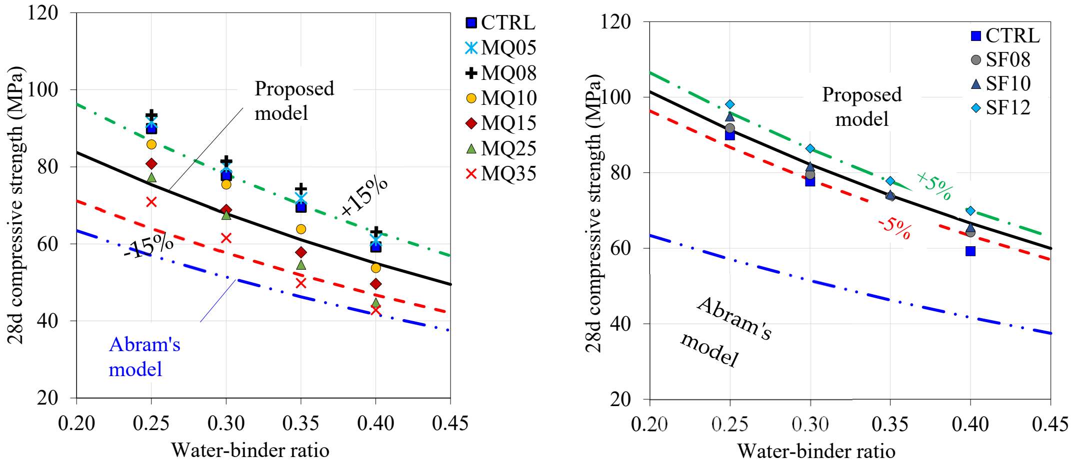

Figure 8. The 28 d compressive strength vs. water–binder ratio: (**a**) MQF, and (**b**) SF concrete.

4.1.3. The Age-Dependent Compressive Strength

A number of factors determine the age-dependent strength of concrete, namely the type of cement used, the type of admixtures used, the water–binder ratio, and weather conditions [65]. The relationship for strength as a function of time assumes moist curing and normal temperature (20 °C). Assuming a constant water–binder ratio, it was predicted that higher strength would be achieved by exposing the cement to moist curing conditions for a prolonged period of time since anhydrous cement particles undergo hydration during drying. The strength of the material does not significantly increase with time after moisture is removed by capillaries under air-curing conditions [66]. After 28 days, silica fume does not significantly increase compression strength (ACI 234-06). The apparent decrease in compressive strength due to the addition of silica fume to concrete over a period of 90 days has been reported in very limited literature [67].

Based on ACI 234, the impact of testing machines on compressive strength may be the cause of the reduction in strength. In this study, the strength experimental observations at various ages are compared with calculated strengths based on the formulas for time-dependent strength provided by ACI Committee 209 (Equation (4)) and CEB-*fib*-90 mode code (Equation (5)). In Figure 9, the compressive strength of MQF concrete is illustrated as a function of age. In the course of the curing process, ultrafine MQF is found to have a positive effect on the strength gain of concrete, even at higher MQF doses. As a result of the hydration of anhydrous cement particles and the very slow hydration of ultrafine quartz particles, a rise in compressive strength can be explained. According to Figure 9, the inclusion of almost 10% MQF in concrete did not adversely affect its strength properties. A possible explanation is that ultrafine grain particles were packed between cement particles in order to achieve maximum compression strength at the microscopic scale. Further, the ultrafine particles provided the greatest increase in compression strength when added to the system later (after 90 days), regardless of the dosage content. At an early stage (up to 28 days) of concrete development, when a water–binder ratio of 0.35 or 0.40 is used (Figure 9c,d), the concrete's compressive strength decreases with an increased dosage of ultrafine MQF.

$$f_c(t) = \left(\frac{t}{4 + 0.85\,t}\right) f_c' \tag{4}$$

$$f_c(t) = \exp\left[s\left(1 - \sqrt{\frac{28}{t/t_1}}\right)\right] f_c' \tag{5}$$

where,

$f_c(t)$: mean compressive strength at age t days.
s: a coefficient that depends on the cement type (0.20 for high early strength, 0.25 for normal hardening, and 0.38 for slow hardening).
t_1: 1 day.

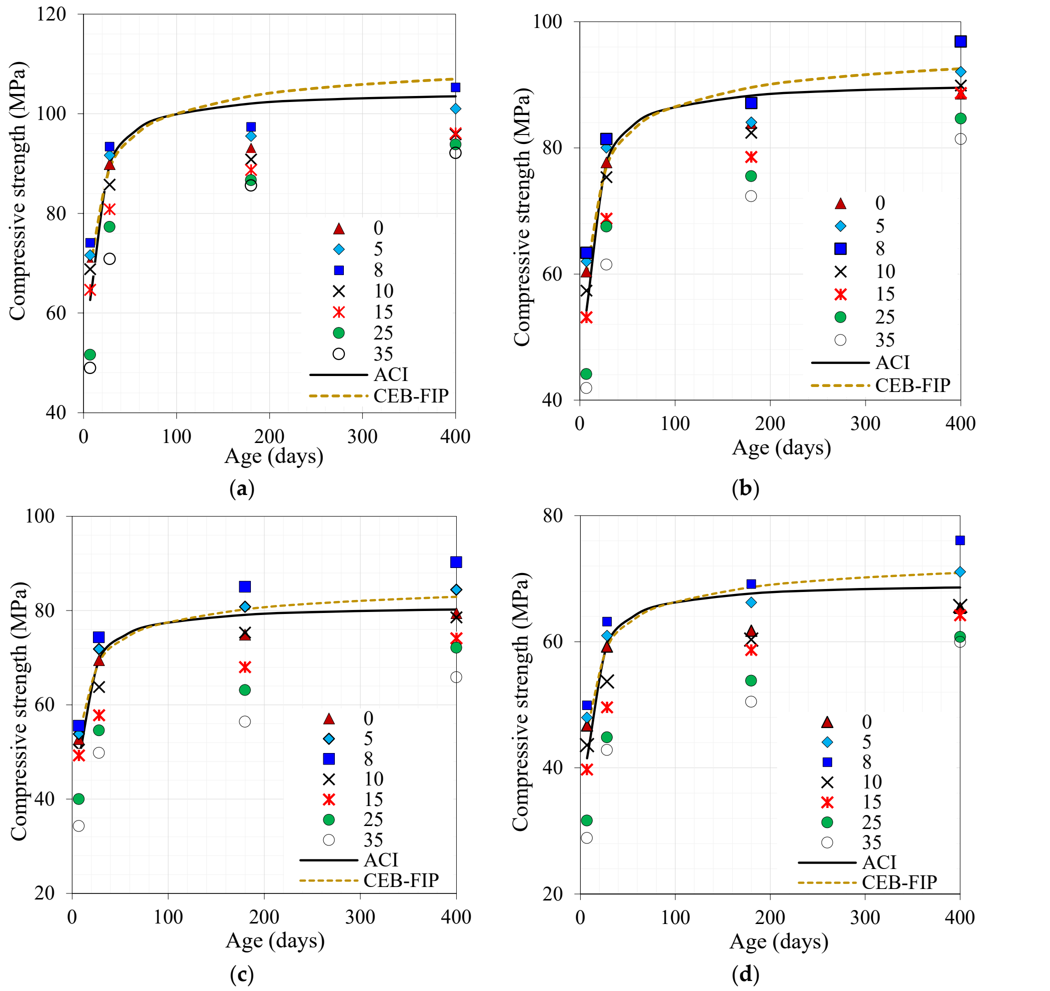

Figure 9. The age-dependent MQF concrete compressive strength development with (**a**) 0.25, (**b**) 0.30, (**c**) 0.35, and (**d**) 0.40 water–binder ratio.

The increase in compressive strength beyond 28 days with the control mix with a water–binder ratio of 0.25 appears to be significantly smaller than that predicted by ACI Committee 209 and CEB-*fib*-90 model codes, as illustrated in Figure 10a. Nevertheless, the ACI-209 and CEB-*fib*-90 models more accurately calculated the compressive strength gains for MQF concrete with a 0.30 water–binder ratio (Figure 10b).

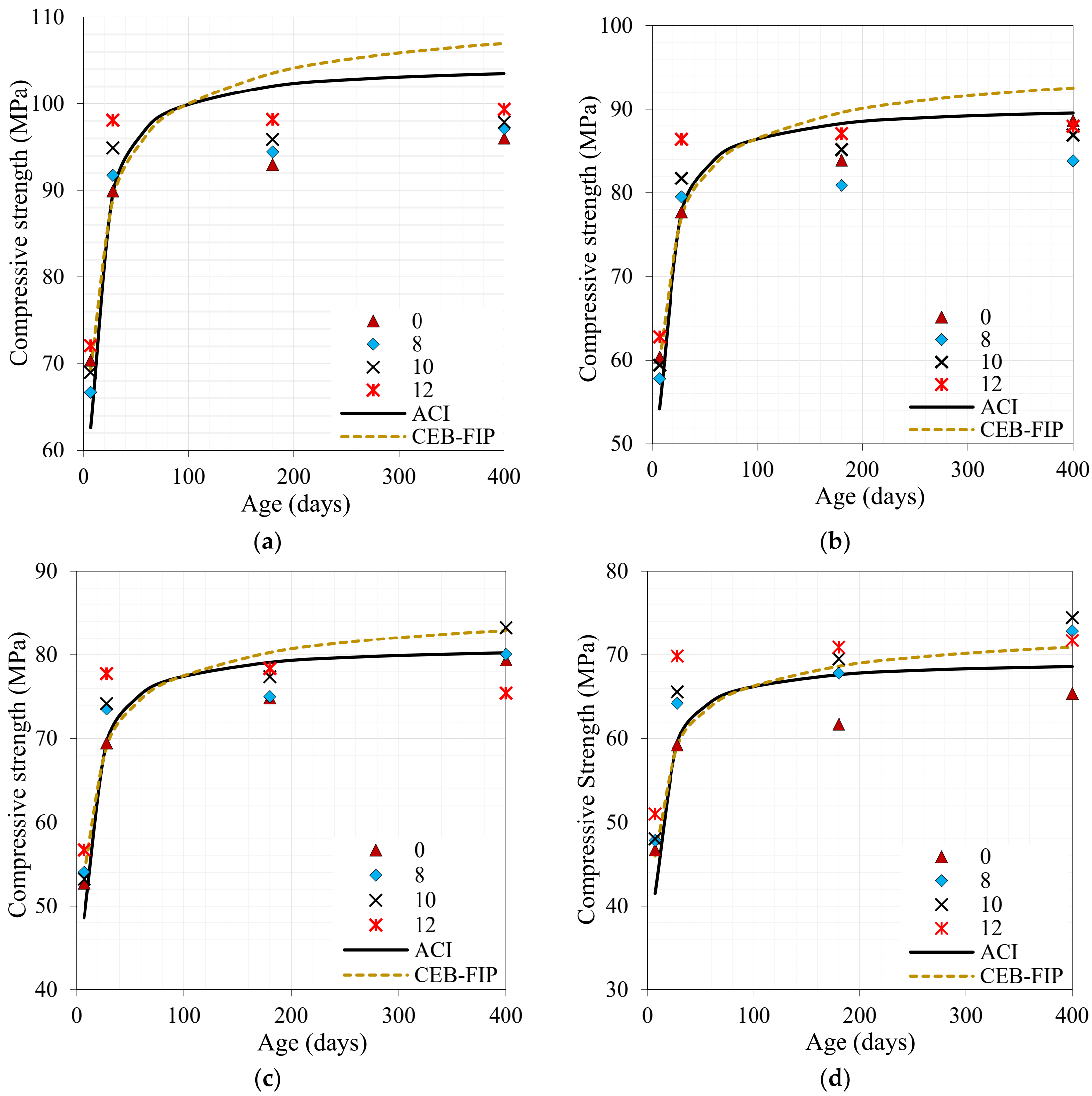

Figure 10. The age-dependent SF concrete compressive strength development with (**a**) 0.25, (**b**) 0.30, (**c**) 0.35, and (**d**) 0.40 water–binder ratio.

Figure 10 shows a plot of the development of the compressive strength of SF concrete with a variety of water–binder ratios. As shown in the figure, the replacement of cement with SF has resulted in a significant increase in the early-age strength of concrete compared to control concrete. In the early stages of SF replacement, strength increases may be attributed to (i) a tighter packing of the particles at the micro-scale, and (ii) a chemical reaction between SF and the cementitious matrix. Further, the ACI-209 and CEB-*fib*-90 predicted the strength of control mixtures nearly perfectly at ages up to 28 days. Nevertheless, at an early age, the compressive strength of SF concrete was higher than that predicted by ACI-209 and CEB-fib-90. Additionally, the compressive strength did not show a significant improvement with aging and was lower than that of the ACI-209 and CEB-FIP models. Several studies [68–70] indicate that many major cement hydration processes occurred during the early stages of cement formation (up to 24 h), which may explain the phenomenon.

In Figure 11, the replacement of cement with MQF and SF ultrafines led to increased compressive strength, indicating a better paste microstructure, which was apparent from the failure pattern. A typical mode of failure was aggregate fractures, regardless of the water–binder ratio. The paste–aggregate with a lower water–cement ratio was more resistant to loading due to stronger bonding and more compacted interfacial transition zones.

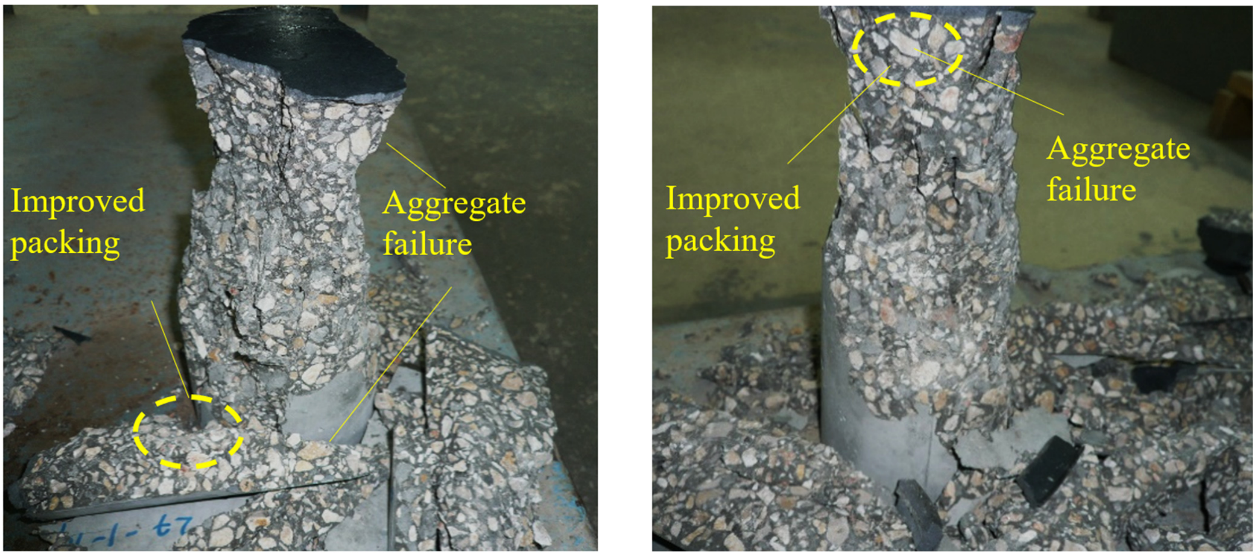

(**a**) (**b**)

Figure 11. Failure patterns during uniaxial compression loading for (**a**) MQF concrete, (**b**) SF concrete.

4.2. Durability Characteristics

4.2.1. The Chloride-Ion Permeability

The rapid-chloride permeability test (RCPT) was conducted according to ASTM C1012. Figure 12 shows the impact of MQF and SF ultrafines on chloride-ion penetration of concrete using different water–binder ratios (0.25–0.40). The ASTM 1202 limits (see Appendix A) of ion transmission are also shown in the figure to illustrate the range of materials through which chloride ions can be transmitted. The figure shows that the passage of charge through the matrix was significantly reduced by increasing the ultrafine dosage. The result can be explained with the filling of pores between cement particles with ultrafine materials, which facilitate enhanced packing of the matrix, resulting in a significant reduction in permeability. This part will be further investigated using the mercury intrusion porosimetry technique as an extension of this work. For the series with MQF, using 8% MQF ultrafines as a matrix, the passing charge through concrete was reduced to below the "low limit" for all water–binder ratios. The charge passing through concrete material was lower than the "very low" limit at the water–binder ratio of 0.3 and with 8% MQF ultrafines. Additionally, 15% MQF ultrafines added to concrete resulted in "very low" concrete permeability, regardless of the water–binder ratio. The permeability of concrete and the dosage of MQF generally follow a logarithmic function, as shown in Figure 12a. On the other hand, the initial and higher dosages of SF were efficient enough to reduce permeability below the very low limit, as shown in Figure 13b.

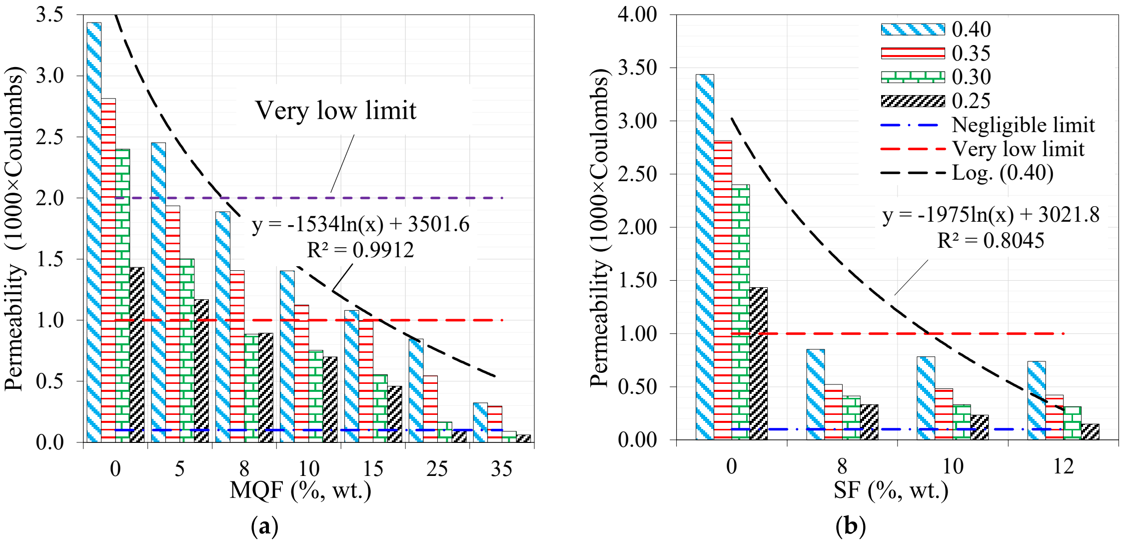

Figure 12. Chloride permeability of (**a**) MQF concrete, and (**b**) SF concrete.

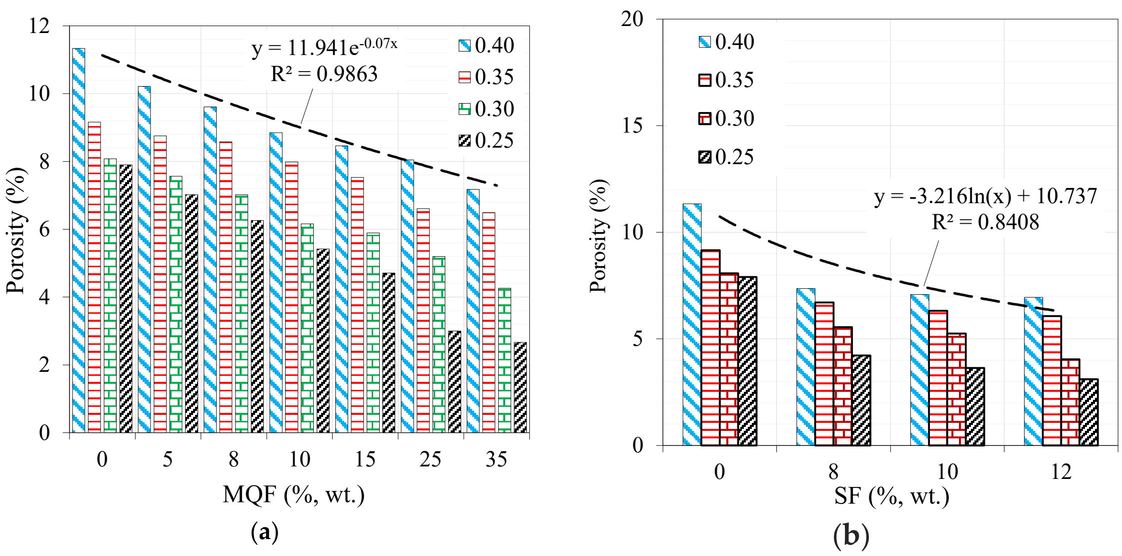

Figure 13. Porosity of (**a**) MQF concrete, and (**b**) SF concrete.

Moreover, a significant reduction in the passing charge through the matrix occurred after the addition of SF was observed in Figure 12b. In all water–binder ratios, adding 8% SF resulted in passing charges through concrete below ASTM 1202's "very low" limit. In addition to being capable of micro-filling concrete, SF also enhances the microstructure of concrete and makes it dense as a result of its pozzolanic reaction. The results of other studies that investigated the pozzolanic effects of SF confirmed this improvement in the microstructure [71–74]. Moreover, the permeability of concrete did not improve significantly with an increase in the SF dosage from 8 to 12%.

4.2.2. The Porosity

Figure 13a illustrates the influence of MQF incorporation into concrete on its porosity at various water–binder ratios. The porosity of concrete mixes with a higher water–binder ratio has been observed to be higher. By increasing the dosage of MQF, a significant reduction in matrix porosity has been observed (Figure 13a). At higher water–binder ratios, adding MQF to concrete mixtures resulted in less porosity improvement, perhaps due to reduced cement content in concrete mixtures and therefore fewer micropores. At lower ratios, however, the improvement in porosity was more pronounced. In general, the porosity of concrete and the MQF dosage were exponentially related (Figure 13a).

At varying water–binder ratios, the impact of the incorporation of SF into concrete on its porosity is illustrated in Figure 13b. As the water–binder ratio increased, the porosity increased throughout the matrix, with the maximum porosity observed at 0.4. A substantial reduction in matrix porosity has also been observed as a result of increased SF content. With higher water–binder ratios, the addition of SF to concrete mixtures resulted in a lesser increase in porosity, which can be attributed to the fewer micropores available since there was less cement in the mixture. The porosity improvement is more significant in mixtures with a lower water-to-cement ratio. The overall trend of a logarithmic function was observed in all mixtures with different levels of substitution of SF.

4.3. Correlations of Different Parameters of Concrete Mixtures

A representation of the strength and permeability responses for the various developed MQF concrete mixtures is shown in Figure 14. Based on the figure, a replacement level of more than 8% MQF led to a reduction in compressive strength. In general, the results indicate that concrete containing 8% MQF and a 0.3 water–binder ratio had improved compressive strength and durability properties. The strength and permeability contours are presented in Figure 15a,b, respectively.

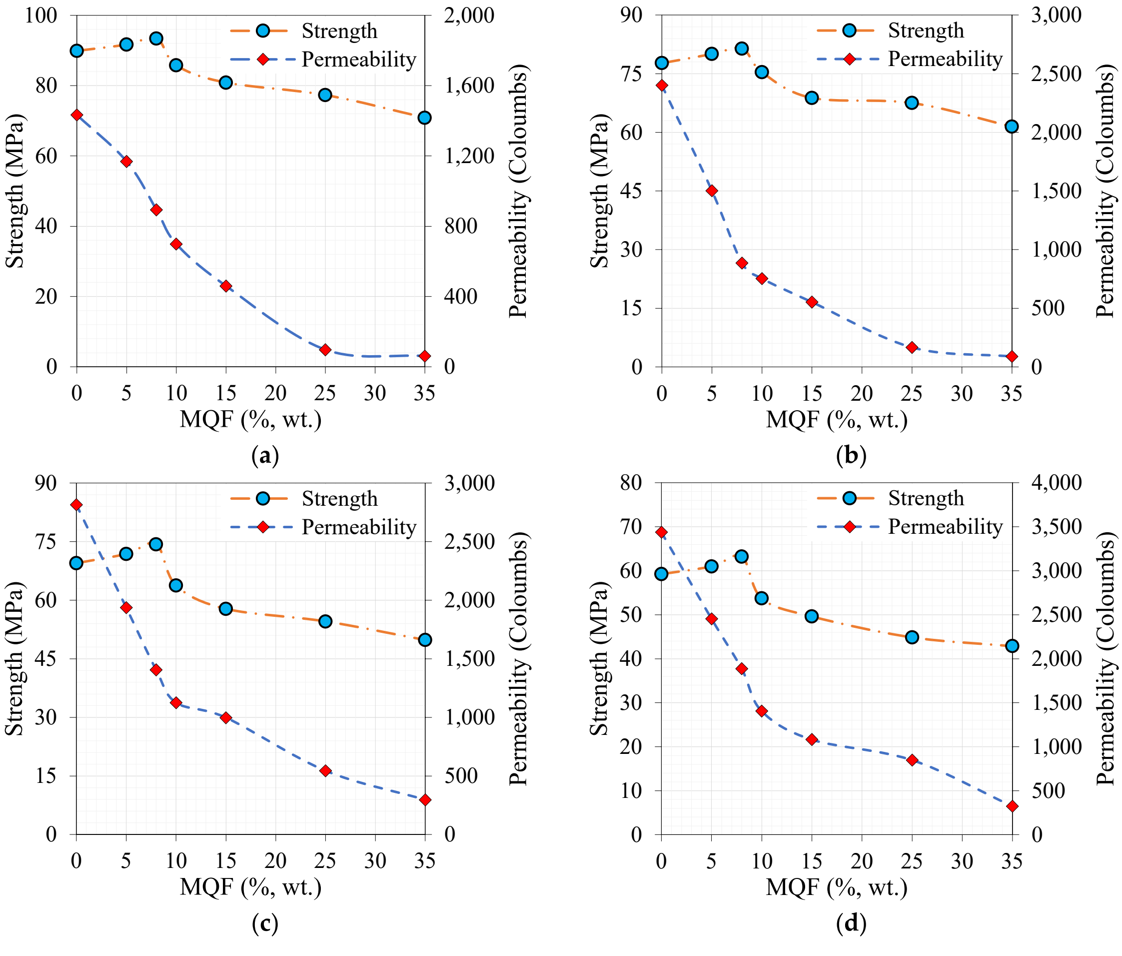

Figure 14. Strength and permeability responses for the various developed MQF concrete mixtures with a w/b ratio of (**a**) 0.25, (**b**) 0.30, (**c**) 0.35, and (**d**) 0.40.

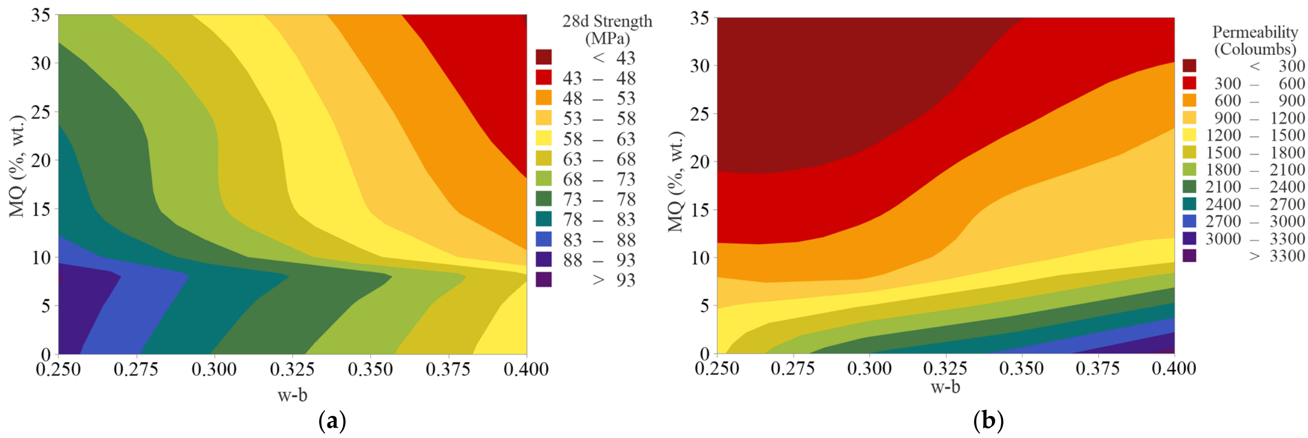

Figure 15. (**a**) Strength and (**b**) permeability contour plots for the MQF concrete mixtures.

5. Conclusions, Limitations, and Future Directions

In this study, we have studied the effects of MQF and SF on the properties of cementitious concrete. The findings offer valuable insights into the behavior of these materials in various concrete mixes with different water–binder ratios. Firstly, we observed that as the replacement level of both MQF and SF rises, there is a consistent decrease in porosity and permeability, irrespective of the type of fine material used. Secondly, with respect to compressive strength, SF displays a notable enhancement, reaching its zenith at an 8% MQF replacement level. Thirdly, the strength of all SF mixes outperformed their MQF counterparts, remaining highest at an 8% MQF replacement level. It is noteworthy that MQF, akin to SF, significantly contributes to compressive strength, porosity reduction, and permeability improvements despite its high crystallinity.

The implications of these findings extend to a range of potential research directions and practical applications. To strike a balance between mechanical properties and cost-effectiveness, further exploration of the optimal SF and MQF replacement proportions is needed. Additionally, the assessment of life cycle and sustainability implications of these cementitious systems should be prioritized. The integration of nanomaterials, such as nano-silica or nano-alumina, in binary cementitious systems represents a promising avenue for future investigations. Moreover, the study of ultrafine fillers derived from inert materials and their impact on the durability of high-strength concrete is a critical area for further exploration. Furthermore, evaluating the influence of MQF and SF proportions on concrete ductility and in-depth assessments of workability and rheological characteristics across a broad spectrum of MQF and SF combinations are essential facets of ongoing research endeavors.

Author Contributions: Conceptualization, M.I.K.; Methodology, G.F.; Software, Y.M.A.; Validation, Y.M.A. and G.F.; Formal analysis, G.F.; Investigation, Y.M.A.; Resources, M.I.K.; Data curation, Y.M.A.; Writing—original draft, M.I.K. and Y.M.A.; Writing—review and editing, Y.M.A. and G.F.; Supervision, M.I.K.; Project administration, M.I.K.; Funding acquisition, M.I.K. All authors have read and agreed to the published version of the manuscript.

Funding: This research was funded by King Saud University, grant number: RSPD2023R692.

Institutional Review Board Statement: Not applicable.

Informed Consent Statement: Not applicable.

Data Availability Statement: Data are contained within the article.

Acknowledgments: The authors extend their appreciation to Researcher Supporting Project number RSPD2023R692, King Saud University, Riyadh, Kingdom of Saudi Arabia.

Conflicts of Interest: The authors declare no conflict of interest.

Appendix A

Limits of RCPT, as outlined in ASTM C1012.

Charge Passed (Coulombs)	Chloride Ion Penetrability
>4000	High
2000–4000	Moderate
1000–2000	Low
100–1000	Very low
<100	Negligible

References

1. Initiative Cement Sustainability (CSI). *Recycling Concrete*; World Business Council for Sustainable Development-WBCSD: Geneva, Switzerland, 2009.
2. Aıtcin, P. The durability characteristics of high performance concrete: A review. *Cem. Concr. Compos.* **2003**, *25*, 409–420. [CrossRef]
3. Stroeven, M. Discrete Numerical Modelling of Composite Materials-Application to Cementitious Materials. Ph.D. Thesis, Civil Engineering and Geosciences, Delft University of Technology, Delft, The Netherlands, 1999.
4. Bai, G.; Wang, L.; Ma, G.; Sanjayan, J.; Bai, M. 3D printing eco-friendly concrete containing under-utilised and waste solids as aggregates. *Cem. Concr. Compos.* **2021**, *120*, 104037. [CrossRef]
5. Zhou, Y.; Guo, D.; Xing, F.; Guo, M. Multiscale mechanical characteristics of ultra-high performance concrete incorporating different particle size ranges of recycled fine aggregate. *Constr. Build. Mater.* **2021**, *307*, 125131. [CrossRef]
6. Bui, D.; Hu, J.; Stroeven, P. Particle size effect on the strength of rice husk ash blended gap-graded Portland cement concrete. *Cem. Concr. Compos.* **2005**, *27*, 357–366. [CrossRef]
7. Zhang, H.; Ji, T.; Liu, H. Performance evolution of the interfacial transition zone (ITZ) in recycled aggregate concrete under external sulfate attacks and dry-wet cycling. *Constr. Build. Mater.* **2019**, *229*, 116938. [CrossRef]
8. Zhao, H.; Wu, Z.; Liu, A.; Zhang, L. Numerical insights into the effect of ITZ and aggregate strength on concrete properties. *Theor. Appl. Fract. Mech.* **2022**, *120*, 103415. [CrossRef]
9. Lagerblad, B.; Kjellsen, K. *Normal and High Strength Concretes with Conventional Aggregates*; RILEM REPORT: Kyoto, Japan, 1999; pp. 53–70.
10. Kaufmann, J.; Winnefeld, F. Influence of addition of ultrafine cement on the rheological properties and strength of Portland cement paste. In *Innovations and Developments in Concrete Materials and Construction, Proceedings of the International Conference Held at the University of Dundee, Scotland, UK, 9–11 September 2002*; Thomas Telford Publishing: London, UK, 2002; pp. 827–836.
11. Bayramov, F.; Tasdemir, M.; Ilki, A.; Yerlikaya, M. Steel fibre reinforced concrete for heavy traffic load conditions. In Proceedings of the 9th International Symposium on Concrete Roads, Istambul, Turkey, 13–16 September 2004; pp. 3–6.
12. Andersen, V.; Einarsrud, K.E.; Rasouli, A.; Tranell, G. Silica Fume Formation in Different Gas Atmospheres. *Ind. Eng. Chem. Res.* **2023**, *62*, 4246–4259. [CrossRef]
13. Neville, A.M. *Properties of Concrete*; Pearson: London, UK, 2004; Volume 4.
14. Dobiszewska, M.; Schindler, A.K.; Pichór, W. Mechanical properties and interfacial transition zone microstructure of concrete with waste basalt powder addition. *Constr. Build. Mater.* **2018**, *177*, 222–229. [CrossRef]
15. Adamu, M.; Ibrahim, Y.E.; Al-Atroush, M.E.; Alanazi, H. Mechanical properties and durability performance of concrete containing calcium carbide residue and nano silica. *Materials* **2021**, *14*, 6960. [CrossRef]
16. Mazloom, M.; Ramezanianpour, A.; Brooks, J. Effect of silica fume on mechanical properties of high-strength concrete. *Cem. Concr. Compos.* **2004**, *26*, 347–357. [CrossRef]
17. Güneyisi, E.; Gesoğlu, M.; Karaoğlu, S.; Mermerdaş, K. Strength, permeability and shrinkage cracking of silica fume and metakaolin concretes. *Constr. Build. Mater.* **2012**, *34*, 120–130. [CrossRef]
18. Shi, H.-s.; Xu, B.-w.; Zhou, X.-c. Influence of mineral admixtures on compressive strength, gas permeability and carbonation of high performance concrete. *Constr. Build. Mater.* **2009**, *23*, 1980–1985. [CrossRef]
19. Behnood, A.; Ziari, H. Effects of silica fume addition and water to cement ratio on the properties of high-strength concrete after exposure to high temperatures. *Cem. Concr. Compos.* **2008**, *30*, 106–112. [CrossRef]
20. Wong, H.; Razak, H.A. Efficiency of calcined kaolin and silica fume as cement replacement material for strength performance. *Cem. Concr. Res.* **2005**, *35*, 696–702. [CrossRef]
21. Barger, G.S.; Hill, R.L.; Ramme, B.W.; Bilodeau, A.; Hooton, R.D.; Ravina, D.; Bury, M.A.; Humphrey, H.J.; Reddy, D.; Carrasquillo, R.L. *Use of Fly Ash in Concrete*; American Concrete Institute: Farmington Hills, MI, USA, 2003.
22. Papadakis, V.G. Effect of fly ash on Portland cement systems: Part I. Low-calcium fly ash. *Cem. Concr. Res.* **1999**, *29*, 1727–1736. [CrossRef]
23. Poon, C.S.; Kou, S.; Lam, L.; Lin, Z. Activation of fly ash/cement systems using calcium sulfate anhydrite ($CaSO_4$). *Cem. Concr. Res.* **2001**, *31*, 873–881. [CrossRef]

24. Russell, M.; Basheer, P.; Rao, J. Potential use of spent mushroom compost ash as an activator for pulverised fuel ash. *Constr. Build. Mater.* **2005**, *19*, 698–702. [CrossRef]
25. Zhang, J.; Lv, T.; Hou, D.; Dong, B. Synergistic effects of fly ash and MgO expansive additive on cement paste: Microstructure and performance. *Constr. Build. Mater.* **2023**, *371*, 130740. [CrossRef]
26. Hanif, A.; Lu, Z.; Li, Z. Utilization of fly ash cenosphere as lightweight filler in cement-based composites–A review. *Constr. Build. Mater.* **2017**, *144*, 373–384. [CrossRef]
27. Khan, M. Permeation of high performance concrete. *J. Mater. Civ. Eng.* **2003**, *15*, 84–92. [CrossRef]
28. Yazıcı, H. The effect of curing conditions on compressive strength of ultra high strength concrete with high volume mineral admixtures. *Build. Environ.* **2007**, *42*, 2083–2089. [CrossRef]
29. Demirboğa, R. Thermal conductivity and compressive strength of concrete incorporation with mineral admixtures. *Build. Environ.* **2007**, *42*, 2467–2471. [CrossRef]
30. Nochaiya, T.; Wongkeo, W.; Chaipanich, A. Utilization of fly ash with silica fume and properties of Portland cement–fly ash–silica fume concrete. *Fuel* **2010**, *89*, 768–774. [CrossRef]
31. Azmee, N.; Abbas, Y.M.; Shafiq, N.; Fares, G.; Osman, M.; Iqbal Khan, M. Enhancing the microstructure and sustainability of ultra-high-performance concrete using ultrafine calcium carbonate and high-volume fly ash under different curing regimes. *Sustainability* **2021**, *13*, 3900. [CrossRef]
32. Abbas, Y.M.; Khan, M.I. Optimization of Arabian-Shield-Based Natural Pozzolan and Silica Fume for High-Performance Concrete Using Statistical Design of Experiments. *Adv. Civ. Eng.* **2021**, *2021*, 5512666. [CrossRef]
33. Abbas, Y. Simplex-lattice strength and permeability optimization of concrete incorporating silica fume and natural pozzolan. *Constr. Build. Mater.* **2018**, *168*, 199–208. [CrossRef]
34. Khan, M.I.; Abbas, Y.M. Curing optimization for strength and durability of silica fume and fuel ash concretes under hot weather conditions. *Constr. Build. Mater.* **2017**, *157*, 1092–1105. [CrossRef]
35. Khan, M.I.; Abbas, Y.M. Robust Extreme Gradient Boosting Regression Model for Compressive Strength Prediction of Blast Furnace Slag and Fly Ash Concrete. *Mater. Today Commun.* **2023**, *35*, 105793. [CrossRef]
36. Bouzoubaa, N.; Bilodeau, A.; Sivasundaram, V.; Fournier, B.; Golden, D.M. Development of ternary blends for high-performance concrete. *Mater. J.* **2004**, *101*, 19–29. [CrossRef]
37. Özyıldırım, C.; Halstead, W. Improved concrete quality with combinations of fly ash and silica fume. *ACI Mater. J.* **1994**, *91*, 587–594.
38. Ronne, M. Effect of condensed silica fume and fly ash on compressive strength development of concrete. *Spec. Publ.* **1989**, *114*, 175–190.
39. Abed, M.; Nemes, R. Long-term durability of self-compacting high-performance concrete produced with waste materials. *Constr. Build. Mater.* **2019**, *212*, 350–361. [CrossRef]
40. Bakker, R. *Application and Advantages of Blended Cement Concretes*; Technical Note; QCL Group: Newstead, Australia, 1999.
41. Moosberg-Bustnes, H.; Lagerblad, B.; Forssberg, E. The function of fillers in concrete. *Mater. Struct.* **2004**, *37*, 74–81. [CrossRef]
42. Nehdi, M. Microfiller Effect on Rheology, Microstructure, and Mechanical Properties of High-Performance Concrete. Ph.D. Thesis, Civil Engineering Department, National Library of Canada = Bibliothèque nationale du Canada, Ottawa, The University of British Columbia, Ottawa, ON, Canada, 1999.
43. Fennis, S. Design of Ecological Concrete by Particle Packing Optimization. Ph.D. Thesis, University of Technology, Delft, The Netherlands, 2011.
44. Vogt, C. Ultrafine Particles in Concrete: Influence of Ultrafine Particles on Concrete Properties and Application to Concrete Mix Design. Ph.D. Thesis, School of Architecture and the Built Environment, Royal Institute of Technology, Stockholm, Sweden, 2010.
45. Cyr, M.; Lawrence, P.; Ringot, E. Mineral admixtures in mortars: Quantification of the physical effects of inert materials on short-term hydration. *Cem. Concr. Res.* **2005**, *35*, 719–730. [CrossRef]
46. Shi, C.; Wu, Z.; Xiao, J.; Wang, D.; Huang, Z.; Fang, Z. A review on ultra high performance concrete: Part I. Raw materials and mixture design. *Constr. Build. Mater.* **2015**, *101*, 741–751. [CrossRef]
47. Mehdipour, I.; Khayat, K.H. Effect of particle-size distribution and specific surface area of different binder systems on packing density and flow characteristics of cement paste. *Cem. Concr. Compos.* **2017**, *78*, 120–131. [CrossRef]
48. Yousuf, S.; Sanchez, L.; Shammeh, S. The use of particle packing models (PPMs) to design structural low cement concrete as an alternative for construction industry. *J. Build. Eng.* **2019**, *25*, 100815. [CrossRef]
49. Kosmatka, S.H.; Kerkhoff, B.; Panarese, W. Fly ash, slag, silica fume, and natural pozzolans. *Des. Control. Concr. Mix.* **2002**, *13*, 57–72.
50. Zagar, L. Methods of determination of pore structure, permeability and diffusion. In Proceedings of the RILEM/IUPAC International Symposium on the Pore Structure and Properties of Materials, Prague, Czech Republic, 18–21 September 1973; pp. C249–C278.
51. Cheerarot, R.; Tangpagasit, J.; Jaturapitakkul, C. Compressive strength of mortars due to pozzolanic reaction of fly ash. *Spec. Publ.* **2004**, *221*, 411–426. [CrossRef]
52. Jaturapitakkul, C.; Tangpagasit, J.; Songmue, S.; Kiattikomol, K. Filler effect and pozzolanic reaction of ground palm oil fuel ash. *Constr. Build. Mater.* **2011**, *25*, 4287–4293. [CrossRef]

53. Khan, M.; Abbas, Y.; Fares, G. Review of high and ultrahigh performance cementitious composites incorporating various combinations of fibers and ultrafines. *J. King Saud Univ.-Eng. Sci.* **2017**, *29*, 339–347. [CrossRef]
54. Wang, X.; Wu, D.; Zhang, J.; Yu, R.; Hou, D.; Shui, Z. Design of sustainable ultra-high performance concrete: A review. *Constr. Build. Mater.* **2021**, *307*, 124643. [CrossRef]
55. Kirthika, S.; Singh, S.; Chourasia, A. Alternative fine aggregates in production of sustainable concrete-A review. *J. Clean. Prod.* **2020**, *268*, 122089. [CrossRef]
56. Loland, K.; Hustad, T. *Report 2 Mechanical Properties*; FCB/SINTEF: Trondheim, Norway, 1981.
57. Sellevold, E.J.; Nilsen, T. Condensed silica fume in concrete: A world review. In Proceedings of the Supplementary Cementing Materials for Concrete CANMET, Ottawa, ON, Canada, 1987; pp. 165–243.
58. Newman, J.; Choo, B.S. *Advanced Concrete Technology 2: Concrete Properties*; Elsevier: Amsterdam, The Netherlands, 2003.
59. Benli, A.; Karataş, M.; Bakir, Y. An experimental study of different curing regimes on the mechanical properties and sorptivity of self-compacting mortars with fly ash and silica fume. *Constr. Build. Mater.* **2017**, *144*, 552–562. [CrossRef]
60. Lamond, J.F.; Pielert, J.H. *Significance of Tests and Properties of Concrete and Concrete-Making Materials*; ASTM International: West Conshohocken, PA, USA, 2006; Volume 169.
61. Scrivener, K.L.; Juilland, P.; Monteiro, P.J. Advances in understanding hydration of Portland cement. *Cem. Concr. Res.* **2015**, *78*, 38–56. [CrossRef]
62. Abrams, L. *Properties of Concrete*; Pitman Publishing Ltd.: London, UK, 1919.
63. Oluokun, F.A. Fly ash concrete mix design and the water-cement ratio law. *Mater. J.* **1994**, *91*, 362–371. [CrossRef]
64. Abd Elaty, M.A.A. Compressive strength prediction of Portland cement concrete with age using a new model. *HBRC J.* **2014**, *10*, 145–155. [CrossRef]
65. Taerwe, L. *Constitutive Modelling of High Strength/High Performance Concrete: State-of-Art Report*; Fédération Internationale du Béton (FIB): Los Santos, SA, USA, 2008; Volume 42.
66. Mehta, P.K.; Monteiro, P.J. *Concrete: Microstructure, Properties, and Materials*; McGraw-Hill Education: New York, NY, USA, 2014.
67. Burg, R.; Ost, B. *Engineering Properties of Commercially Available High-Strength Concretes (Including Three-Year Data)*; The National Academies of Sciences, Engineering, and Medicine: Washington, DC, USA, 1994.
68. Hu, J.; Ge, Z.; Wang, K. Influence of cement fineness and water-to-cement ratio on mortar early-age heat of hydration and set times. *Constr. Build. Mater.* **2014**, *50*, 657–663. [CrossRef]
69. Qi, T.; Zhou, W.; Liu, X.; Wang, Q.; Zhang, S. Predictive hydration model of Portland cement and its main minerals based on dissolution theory and water diffusion theory. *Materials* **2021**, *14*, 595. [CrossRef]
70. Shen, D.; Wang, X.; Wu, S. Determining hydration mechanisms for initial fall and main hydration peak in tricalcium silicate hydration using a two-scale hydration simulation model. *Cem. Concr. Res.* **2022**, *156*, 106763. [CrossRef]
71. Detwiler, R.J.; Mehta, P.K. Chemical and physical effects of silica fume on the mechanical behavior of concrete. *Mater. J.* **1989**, *86*, 609–614. [CrossRef]
72. Goldman, A.; Bentur, A. Properties of cementitious systems containing silica fume or nonreactive microfillers. *Adv. Cem. Based Mater.* **1994**, *1*, 209–215. [CrossRef]
73. Ibrahim, R.K.; Hamid, R.; Taha, M. Strength and Microstructure of Mortar Containing Nanosilica at High Temperature. *ACI Mater. J.* **2014**, *111*, 163–170. [CrossRef]
74. Amin, M.; Zeyad, A.M.; Tayeh, B.A.; Agwa, I.S. Effect of ferrosilicon and silica fume on mechanical, durability, and microstructure characteristics of ultra high-performance concrete. *Constr. Build. Mater.* **2022**, *320*, 126233. [CrossRef]